Bulletin of the Seismological Society of America, Vol. 95, No. 5, pp. 1841–1855, October 2005, doi: 10.1785/0120040181

Global Observational Properties of the Critical Earthquake Model

by C. B. Papazachos, G. F. Karakaisis, E. M. Scordilis, and B. C. Papazachos

Abstract The preshock (critical) regions of 20 mainshocks with magnitudes between 6.4 and 8.3, which occurred recently (since 1980) in a variety of seismotectonic regimes (Greece, Anatolia, Himalayas, Japan, California), were identified and investigated. All these strong earthquakes were preceded by accelerating time-to-mainshock seismic crustal deformation (Benioff strain). The time variation of the cumulative Benioff strain follows a power law with a power value ($m = 0.3$) in very good agreement with theoretical considerations. We observed that the dimension of the critical region increased with increasing mainshock magnitude and with decreasing long-term seismicity rate of the region. An increase of the duration of this critical (preshock) phenomenon with decreasing long-term seismicity rate was also observed. This spatial and temporal scaling expresses characteristics of the critical earthquake model, which are of importance for earthquake prediction research. We also showed that the critical region of an oncoming mainshock coincides with the preparing region of this shock, where other precursory phenomena can be observed.

Introduction

The critical earthquake model is based on principles of statistical physics and has been proposed (Sornette and Sornette, 1990; Allegre and Le Mouel, 1994; Sornette and Sammis, 1995) to explain accelerating intermediate magnitude seismicity observed before strong mainshocks (Tocher, 1959; Mogi, 1969; Varnes, 1989; Sykes and Jaume, 1990; Knopoff *et al.*, 1996; Tzanis *et al.*, 2000; among others). According to this model, the physical process of generation of these moderate magnitude shocks (preshocks) is considered a critical phenomenon, culminating in a large event (mainshock), which is considered as the critical point. Such behavior has been also supported by independent observations, which suggest that rupture in heterogeneous media is a critical phenomenon (Vanneste and Sornette, 1992; Lamaignere *et al.*, 1996; Andersen *et al.*, 1997). Thus, the critical earthquake model is now supported by seismological observations, by principles of statistical physics, and rock mechanics experiments.

Several researchers have recently investigated properties of the model (Bufe and Varnes, 1993; Bowman *et al.*, 1998; Brehm and Braile 1999; Jaume and Sykes, 1999; Rundle *et al.*, 2000). Bufe and Varnes (1993) proposed a power law for the time variation of the cumulative Benioff strain, S (square root of energy), released by preshocks in the critical region:

$$S = A + B(t - t_c)^m \qquad (1)$$

where t_c is the failure time (origin time of the mainshock) and A, B, and m are model parameters. Bowman *et al.* (1998) quantified the degree of deviation of the time variation of S from linearity by proposing the minimization of a curvature parameter, C, which is defined as the ratio of the root mean square error of the power-law fit (relation 1) to the corresponding linear fit error, and showed that the size of the accelerating (critical) region scales with the mainshock magnitude. Similar results were independently obtained by Brehm and Braile (1998, 1999) and supported by mining-induced seismicity and laboratory experiments (Quillon and Sornette, 2000; Johansen and Sornette, 2000). Furthermore, Zoller *et al.* (2001) and Zoller and Hainzl (2002) have performed systematic spatiotemporal tests in an attempt to quantify the predictive power of accelerated deformation release and the related growing of the spatial correlation length. Despite the fact that the critical earthquake concept has been questioned regarding the robustness of the reported analyses (Gross and Rundle, 1998), several theoretical approaches (Ben-Zion *et al.*, 1999; Rundle *et al.*, 2000; Ben-Zion and Lyakhovsky, 2002), as well as laboratory results (Guarino *et al.*, 1999, 2002) have verified the existence of critical behavior, at least under some conditions.

Papazachos and Papazachos (2000, 2001) suggested the use of elliptical critical regions and several constraints to the critical earthquake model expressed by relations between parameters of the accelerating Benioff strain (seismic crustal deformation) and the long-term mean rate of the seismic deformation (seismicity release rate). As a representative measure of the seismicity/seismic deformation, they used the average annual Benioff strain rate in the critical region, S_r (in $J^{1/2}$/yr), as this is determined from the cumulative, long-

term Benioff strain release for events with $\mathbf{M} \geq 5.2$. The use of this specific cutoff magnitude value was imposed by the fact that such events are usually available for a long-time interval (in some areas almost for the whole twentieth century) for many seismogenic regions worldwide, allowing the reliable determination of the average seismic release rate for each examined critical region. The most important of these constraint relations are: (1) A relation between the logarithm of the radius R (in km) of the circle with area equal to the area of the elliptical critical region and the magnitude $\mathbf{M}$ (moment magnitude) of the mainshock; (2) a relation between the logarithm of the duration t_p (in years) of the preshock sequence (that is, of the duration of the accelerating seismic deformation) and the logarithm of the long-term rate of seismic crustal deformation per unit area, S_r (in $J^{1/2}$/yr and per 10 km^2); (3) a relation between the $\log(A/t_p)$ and $\log S_r$, where A is the constant of relation (1); and (4) a relation between the magnitude of the mainshock, $\mathbf{M}$, and the mean magnitude of the three largest preshocks, $\mathbf{M}_{13}$.

Observations for 18 mainshocks of the Aegean area (Papazachos *et al.*, 2002a, b) showed that preshock accelerating deformation can be identified in all cases with $C \leq 0.6$ and $m \leq 0.35$. The C cutoff value observed for the Aegean is slightly smaller than the cutoff value used by Bowman *et al.* (1998). The average observed value for m for the Aegean area is 0.3 (Papazachos *et al.*, 2001), in accordance with theoretical considerations and a large number of worldwide observations (see Ben-Zion and Lyakhovsky [2002] for an indicative summary of results from various studies). Papazachos and Papazachos (2001) defined a parameter P as the average value of the probability that each of the four parameters (R, t_p, A, M) attains a value close to its expected one. Furthermore, Papazachos *et al.* (2002a) chose a quality index, q, defined by the relation

$$q = \frac{P}{mC} \tag{2}$$

in an attempt to simultaneously evaluate the compatibility of an investigated accelerating seismic deformation with the behavior of past real preshock sequences (large P), the degree of seismic acceleration (small m), and the fit of the data to the power law (small C). From the investigation of the same sample of 18 preshock sequences in the Aegean area, the cutoff values of $P \geq 0.45$ and $q \geq 3.0$ have also been determined (Papazachos *et al.*, 2002a,b).

The main target of the present work is to investigate properties of critical regions in active areas with different seismotectonic conditions (Greece, Anatolia, Himalayas, Japan, California) by using the most recent and reliable data. Furthermore, an attempt is made to derive globally valid relations between model parameters that can be used as additional constraints to the critical earthquake model. It is shown that such work supports the validity of the critical earthquake model and can contribute to the improvement of methodology for intermediate-term earthquake prediction, since certain basic properties of the model have a premonitory character for the oncoming mainshock.

The terms "preshocks" and "postshocks" are used in the present article in their broad sense. Thus, while foreshocks and aftershocks are spatially distributed in or near the fault (rupture) zone of the mainshock, and the duration of their sequences is of the order of months, preshocks and postshocks are distributed in a broader region, with dimensions that are typically an order of magnitude larger than the fault length of the mainshock, while the duration of preshock and postshock sequences is of the order of years or decades.

The choice of the critical region shape is of importance for the identification of such regions, and several shapes such as circular (e.g., Bufe and Varnes, 1993; Bowman *et al.*, 1998), elliptical (e.g., Papazachos and Papazachos 2000, 2001), predicted stress-drop pattern (e.g., Bowman and King, 2001) have been used. Circular ones, traditionally used in most studies, have the advantage that the probability that parts of more than one preshock (critical) region will be included in such a shape is small. There are, however, several elongated seismic zones for which no solutions can be found using circular critical regions and reliable solutions are found only for elongated shapes (e.g., elliptical). This is either due to data limitations and critical region overlap or to the real necessity to use ellipses to approximate the true critical region, which some studies have suggested have complicated shapes (e.g., Bowman and King, 2001). Unfortunately, elliptical regions include two additional degrees of freedom (ellipticity, azimuth), hence increasing the probability of finding valid solutions even in random catalogs (e.g., Papazachos *et al.*, 2002a). For this reason, identification of a critical region in a broad area must be tested for both circular and elliptical shapes. Thus, for the 20 preshock sequences studied in the present paper, for 16, both circular and elliptical shapes gave valid solutions, while for the remaining 4 cases, which concern preshock sequences in elongated seismic regions, only elliptical shapes gave valid solutions.

Data and Procedure

Three samples of data are used for each of the five areas considered in the present article. The first sample concerns the mainshocks, the second the preshocks of each mainshock, and the third one includes the shocks that define the long-term mean seismicity in each critical region. Each sample must be complete (including all shocks that occurred during a certain time period with magnitudes larger than a certain value), large enough (to be representative) and accurate (a property that is better satisfied for recent earthquakes). These properties differ from area to area; hence, each area of interest was examined separately.

The main target of the data processing procedure was to obtain homogeneous catalogs exhibiting similar characteristics for all examined areas. For this reason, all magni-

tudes of earthquakes included in the final catalogs are moment magnitudes or equivalent to moment magnitudes, that is, magnitudes that have been converted to moment magnitudes from other scales (i.e., M_s, m_b published by ISC and/or NEIC) by using appropriate formulas and/or graphs proposed by Scordilis (2005). The finally adopted magnitude for each earthquake is the weighted mean of the values calculated by the above transformations by taking as weight for each magnitude value the inverse of the standard deviation, σ, of the corresponding transformation formula. A similar procedure was successfully applied in order to create a homogeneous earthquake catalog, which was used in a retrospective study of accelerated crustal deformation in the Adriatic (Scordilis *et al.*, 2004).

An example of the adopted procedure is shown in Figure 1a, where the equivalent moment magnitude, M_W^*, computed from other magnitudes (M_S, m_b, M_L) is plotted against original M_W determinations for more than 700 events in California for which both estimates were available. In general a very good correlation between the two magnitudes is observed with the standard error being less than 0.2, suggesting that the equivalent moment magnitude can be reliably used in the present study.

Furthermore, in all cases the data completeness has been checked using both, the frequency–magnitude distribution and the cumulative frequency–magnitude relation. Several time periods have been tested to assure the data completeness for each region. For instance, the data completeness for the broader Himalayas area for the time period from 1965 until 2003 has been checked for seven subperiods. It has been finally determined that the data are complete for earthquakes of $\mathbf{M} \geq 4.7$ since 1965 and $\mathbf{M} \geq 4.2$ since 1981 (Fig. 1b and 1c).

In order to ensure the reliability of the data set used, only mainshocks that occurred during the last two decades or so (1980–2002) were considered. The starting time was changed to 1981 for Greece (date of full operation of the first digital telemetric network in Greece) and 1990 for the Himalayas, which is the only area for which a regional catalog source was not available; hence we limited the search to the last decade in order to use the most reliable mainshock–preshock–postshock information.

The main sources of all the catalogs used in the present work were the bulletins of the International Seismological Centre (ISC, 2005) and of the National Earthquake Information Center (NEIC, 2005), as well as the CMT solutions catalog of Harvard (Harvard Seismology, 2005), which were used to create the master catalog for each area until the end of 2002. Using this master catalog for the Himalayas and surrounding area (20°N–45°N, 60°E–90°E) four mainshocks with $\mathbf{M} \geq 7.0$ that occurred since 1990 were considered. The final data sample used concerns shocks with $\mathbf{M} \geq 4.7$ that occurred since 1965.

However, for several of the examined areas, we also used individual catalogs available mainly from reliable local sources, which were merged with the master catalog. Specifically, for the Mediterranean region (Greece and Anatolia, 28°N–55°N, 15°W–46°E), data from the catalogs of European earthquakes compiled by Karnik (1996), which was complemented by the catalog of Papazachos *et al.* (2003) for earthquakes in Greece and surrounding areas, as well as the bulletins of National Observatory of Athens and the Geophysical Laboratory of the University of Thessaloniki have been used. Using the final catalog for the area of Greece and surrounding region (34°N–42°N, 19°E–28°E), all six mainshocks with $\mathbf{M} \geq 6.4$ that occurred between 1981 and 2002 were considered. The following three complete samples of data have been used: 1911–2002, $\mathbf{M} \geq 5.2$ (used for calculation of the mean seismic deformation); 1950–2002, $\mathbf{M} \geq 5.0$; 1965–2002, $\mathbf{M} \geq 4.5$ (used for estimation of the preshock seismic deformation). Similarly, for Anatolia (35°N–42°N, 28°E–42°E), three mainshocks that occurred during the last decade with magnitude $\mathbf{M} \geq 6.4$ were considered. The following three complete samples have been used: 1911–2002, $\mathbf{M} \geq 5.2$; 1950–2002, $\mathbf{M} \geq 5.0$; 1965–2002, $\mathbf{M} \geq 4.5$.

For the area of Japan (30°N–50°N, 130°E–150°E), the catalog has been enriched with data of the Japan Meteorological Agency (JMA), in order to obtain additional information for low-magnitude earthquakes. Four mainshocks with $\mathbf{M} \geq 7.3$ that occurred since 1980 were considered. Examination of completeness showed that the data were complete for $\mathbf{M} \geq 5.0$ since 1926.

Finally, for California (33°N–42°N, 125°W–114°W), additional data from NEIC regarding significant U.S. earthquakes, as well as moment magnitudes from the USGS (Earthquake Hazards Program) have also been used. Furthermore, additional data have been extracted from the Advanced National Seismic System (ANSS) composite earthquake catalog (http://quake.geo.berkeley.edu/anss), which includes contributions from the Southern California Seismic Network, the Seismographic Station of the University of California at Berkeley, and the Northern California Seismic network, among other contributing members. Earthquake magnitudes for California in the ANSS catalogue are given in various scales (M_s, m_b, M_L, M_w, M_c, M_d, etc.). For example, about 65% of the $\mathbf{M} \geq 3.0$ events have M_L or M_c (which is essentially equal to M_L, [Felzer *et al.*, 2002]) magnitudes. All magnitudes were also converted to equivalent moment magnitudes using appropriate relations (Scordilis, 2005). Finally, four mainshocks with $\mathbf{M} \geq 7.0$ that occurred since 1980 were considered, while the examination for completeness showed that the data were complete for $\mathbf{M} \geq 4.8$ since 1930.

The involved uncertainties are typically less than 30 km for the epicenter and less than 0.3 for the equivalent moment magnitude. Therefore, for 20 normal-depth mainshocks that occurred since 1980 and had magnitudes between 6.4 and 8.3 (Table 1), reliable data (magnitude, epicenters of preshocks, etc.) were available, and these data are used to define parameters of their critical (preshock) regions. Although a few preliminary results for some intermediate-depth events

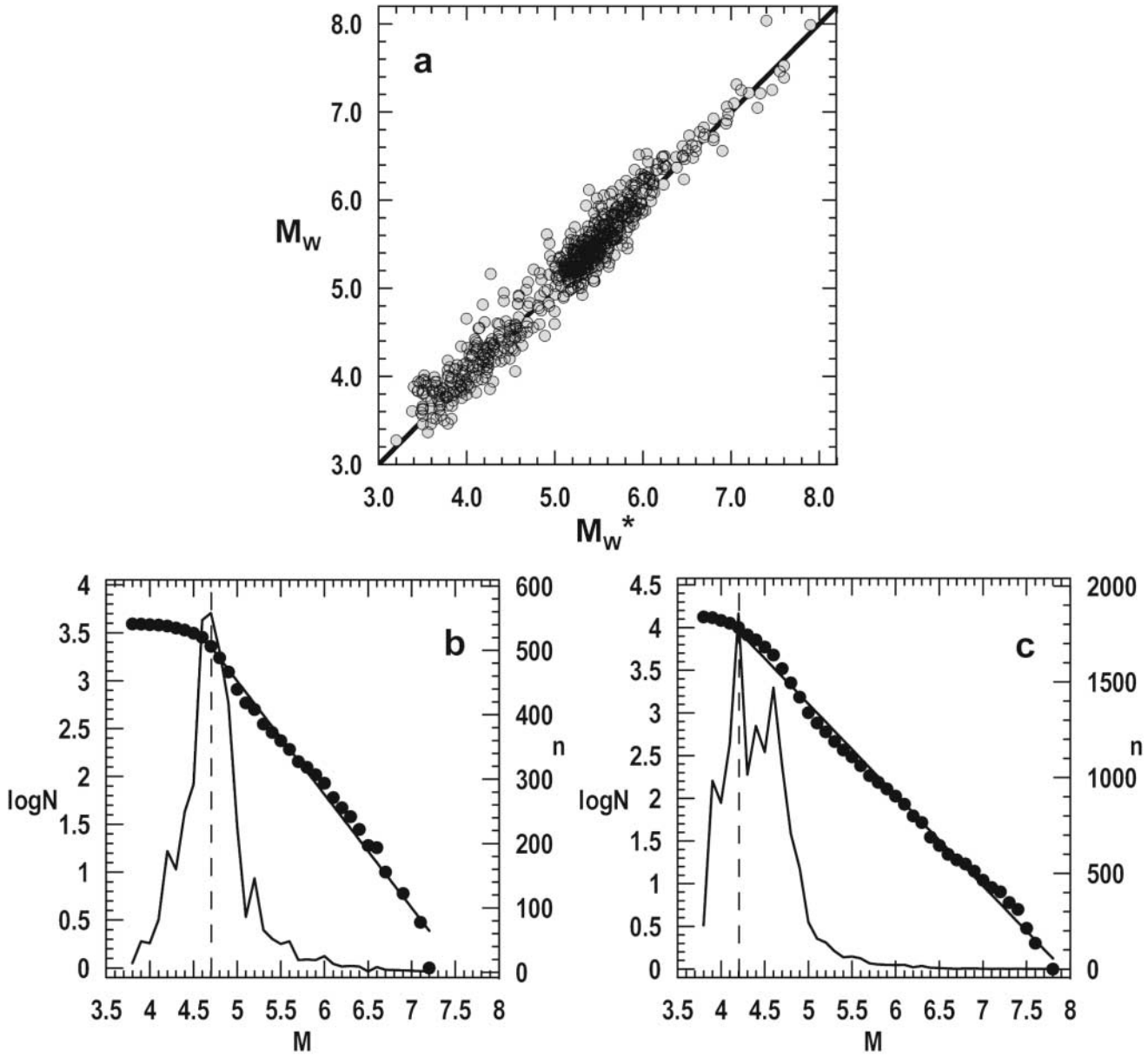

Figure 1. (a) Comparison of the equivalent moment magnitudes, M_W^*, determined from various magnitude sources (M_S, m_b, M_L) with original M_W estimations using the relations of Scordilis (2005) for the catalog used for the broader California area. (b, c) Frequency–magnitude and cumulative frequency–magnitude distributions used for the Himalayas area to define the data completeness for two time periods: 1965–1980 (b) and 1981–2003 (c).

indicate that they also exhibit a similar accelerated deformation preshock behavior, we decided to exclude them from the present work owing to the limited number of associated preshocks, as well as their special characteristics, and leave their study for future work.

To identify an elliptical critical (preshock) region of an already occurred mainshock, the algorithm of Papazachos (2001) has been used. According to this algorithm, the broad seismic zone (e.g., of dimensions 400 km × 400 km), where the mainshock is located (e.g., Hokkaido zone in Japan) is divided using a grid with the desired density (e.g., 0.2° NS, 0.2° EW). Each point of the grid is considered as the center of the elliptical (or circular) critical region, and magnitudes of shocks (preshocks) with epicenters in this region are used to calculate parameters of relation (1) and the curvature parameter C. Calculations for each point of the grid are repeated for a large set of values for the azimuth, z, of the large ellipse axis, its length, a, ellipticity, e, the start time, t_s, of the preshock sequence, the minimum preshock magnitude, M_{min}, and the magnitude of the mainshock (starting

Table 1

Information on the Dates, Geographic Coordinates of the Epicenter, *E*, and Magnitudes of the 20 Mainshocks for which Data Have Been Used in the Present Study

Area		Date (t_c)	$E(\phi, \lambda)$	M	$Q(\phi_1, \lambda_1)$
Greece	1	1981, 02, 24	38.2, 22.9	6.7	40.8, 21.9
	2	1981, 12, 19	39.0, 25.3	7.2	41.0, 22.8
	3	1983, 01, 17	38.1, 20.2	7.0	39.0, 19.8
	4	1995, 05, 13	40.2, 21.7	6.6	38.8, 21.0
	5	1995, 06, 15	38.4, 22.2	6.4	38.7, 21.2
	6	1997, 11, 18	37.6, 20.6	6.6	39.4, 21.1
Anatolia					
	7	1995, 10, 01	38.1, 30.2	6.4	38.4, 28.8
	8	1999, 08, 17	40.8, 30.0	7.4	39.6, 28.2
	9	2002, 02, 03	38.7, 31.2	6.5	38.6, 29.6
Himalayas					
	10	1992, 08, 19	42.1, 73.6	7.2	41.4, 72.2
	11	1997, 02, 27	30.0, 68.2	7.1	26.8, 66.2
	12	1997, 11, 08	35.1, 87.4	7.5	35.0, 90.8
	13	2001, 01, 26	23.4, 70.3	7.6	26.4, 72.2
Japan					
	14	1983, 05, 26	40.4, 139.1	7.7	40.2, 139.4
	15	1993, 07, 12	42.8, 139.2	7.7	41.2, 141.0
	16	1994, 10, 04	43.7, 147.7	8.3	44.6, 146.4
California					
	17	1980, 11, 08	41.1, 124.6	7.3	38.4, 125.2
	18	1989, 10, 18	37.0, 121.9	7.0	38.0, 117.0
	19	1992, 04, 25	40.3, 124.2	7.2	38.9, 122.4
	20	1992, 06, 28	34.2, 116.4	7.3	34.8, 120.8

The geographic coordinates are also given for the point, *Q*, which corresponds to the best solution and is considered as the center of the critical region.

typically from 6.2, up to the magnitude of the largest earthquake in the zone). Calculations were initially performed with variable m value, allowing a wide range of m values between 0.1 and 0.5. The final calculations were made using a constant m value equal to 0.3, as this was determined from the average m value, in very good agreement with theoretical values and laboratory results ranging between 0.25–0.33 (Ben-Zion *et al.*, 1999; Guarino *et al.*, 1999; Rundle *et al.*, 2000; Ben-Zion and Lyakhovsky, 2002) and standard practice in similar studies (e.g., Zoller and Hainzl, 2002; Rundle *et al.*, 2003). All grid points with valid solutions (using the cutoff determined for the Aegean area, $C \leq 0.60$, with $m_{\text{fixed}} = 0.30$, and a minimum number of 20 preshocks) are considered and the geographical point, Q, with the smallest C value was considered as the center of the critical region, while the solution (q, C, M, a, z, e, M_{min}, n, t_s) for this point was adopted as the best solution. The application of this algorithm was repeated for all 20 cases by considering circular regions, and it was found that the results are very similar for 16 cases. For this reason, the solution for the simplest shape (circular) was adopted in these 16 cases. For the other four cases, no valid solutions were found when circular shapes were used. For this reason, the best elliptical solution for each of these four cases was adopted. One of these cases concerns a mainshock along the elongated zone of north Anatolia (case with code number 8 in Tables 1 and 2, with ellipticity $e = 0.9$ and major-axis azimuth $z = 60°$), and three concern mainshocks in the Indian plate boundary (case 10 with $e = 0.9$, $z = 0°$; case 11 with $e = 0.7$, $z = 120°$; and case 12 with $e = 0.7$, $z = 0°$).

Results

Application of the previously described algorithm for the 20 critical regions resulted in the calculation of appropriate model parameters, which are listed in Tables 1 and 2. These parameters can be used to derive several empirical relations. Figures 2–6 show the critical regions (circular or elliptical), while the inset figures show the corresponding time variations of the cumulative Benioff strain.

From the estimated values of $\mathbf{M}^*$ and the minimum preshock magnitude, $\mathbf{M}_{\text{min}}$ (Table 2) for which the best solution (smallest C value) was obtained, the following relation can be derived (Fig. 7):

$$\mathbf{M}^* - \mathbf{M}_{\text{min}} = 0.54\mathbf{M}^* - 1.92, \quad \sigma = 0.08, \quad (3)$$

which is similar to the equation obtained by Papazachos (2003). We made a further attempt to examine the effect of the variation of the minimum preshock magnitude on the results, and we observed that for each mainshock there was a lower as well as a higher cutoff minimum preshock magnitude for which valid solutions ($C < 0.60$, $m_{\text{fixed}} = 0.3$) still existed. Thus, for the Japanese mainshock of 4 October 1994, **M** 8.3, valid solutions were obtained only for $\mathbf{M}_{\text{min}}$ between 5.5 and 5.9. The higher minimum-magnitude limit was clearly a result of the minimum number of preshocks (typically 20), which we imposed in the optimization procedure in order to ensure the reliability of the obtained results (Papazachos and Papazachos, 2000, 2001). Furthermore, the lower minimum magnitude verifies the theoretical results (Rundle *et al.*, 2000), as well as independent observations (e.g., Jaume, 2000; Karakaisis *et al.*, 2002) that such a minimum magnitude exists as a slope change above $\mathbf{M}_{\text{min}}$ in the Gutenberg–Richter distribution during the preshock period. Equation (3) verifies that it is the accelerating generation of intermediate-magnitude preshocks that characterizes the critical phenomenon. This observation also explains why the time variation of the crustal deformation (Benioff strain) better expresses the critical phenomenon (Bufe and Varnes, 1993) than other quantities, such as the frequency of shocks, which is dominated by a large number of small shocks, or the seismic moment, which is dominated by the magnitudes of the largest preshocks.

Extending the initial results of Bowman *et al.* (1998), Papazachos and Papazachos (2000) have shown that the radius, R (in km), of the circle with area equal to the area of the elliptical critical region, scales with the magnitude, **M**, of the mainshock according to a relation of the form:

$$\log R = 0.42\mathbf{M} + a_m \quad (4)$$

Table 2
Information on the Critical Regions of the 20 Mainshocks

Area		**M***	C	q	A	R	$\mathbf{M}_{13}$	log S_r	Log s_r	$\mathbf{M}_{min}$	n	t_s	t_i
Greece	1	7.0	0.43	4.6	0.16	247	6.4	7.18	5.90	5.1	33	1972	1980.7
	2	7.4	0.41	6.0	0.40	368	6.8	7.38	5.91	5.4	41	1969	1980.7
	3	7.4	0.44	6.1	0.52	348	6.8	7.50	5.87	5.4	42	1968	1980.7
	4	6.6	0.35	7.9	0.21	167	6.0	7.21	6.27	4.9	48	1984	1993.1
	5	6.5	0.57	4.6	0.18	139	6.0	7.13	6.35	4.9	43	1984	1993.0
	6	6.9	0.45	6.5	0.34	216	6.4	7.31	6.15	5.1	60	1984	1994.8
Anatolia													
	7	6.4	0.24	8.8	0.13	207	5.8	7.01	5.88	4.9	39	1983	1993.0
	8	7.4	0.25	7.0	0.96	621	6.8	7.88	5.80	5.2	124	1986	1996.9
	9	6.6	0.49	4.7	0.21	234	6.1	6.93	5.69	4.9	62	1981	1995.9
Himalayas													
	10	6.9	0.42	5.0	0.39	373	6.2	7.39	5.75	5.1	69	1979	1990.4
	11	7.1	0.59	5.4	0.34	447	6.5	6.91	5.11	5.2	43	1962	1990.7
	12	7.2	0.44	4.6	0.31	454	6.3	6.86	5.05	5.2	37	1961	1994.9
	13	7.6	0.49	5.2	0.49	735	7.0	7.09	4.89	5.5	42	1956	1992.4
Japan													
	14	7.7	0.52	5.3	0.67	393	7.2	8.02	6.43	5.5	76	1972	1981.6
	15	7.5	0.47	5.2	0.12	336	7.1	8.03	6.48	5.1	180	1984	1990.8
	16	8.1	0.46	4.9	2.60	614	7.5	8.35	6.32	5.6	121	1983	1993.2
California													
	17	6.9	0.36	5.0	0.69	356	6.1	6.87	5.59	5.1	32	1962	1977.1
	18	7.1	0.34	8.3	0.52	458	6.4	7.22	5.48	5.1	84	1962	1983.5
	19	7.6	0.48	5.9	0.98	726	7.1	7.46	5.39	5.5	86	1964	1984.3
	20	7.3	0.32	7.8	0.90	529	6.7	7.35	5.50	5.3	89	1955	1988.3

M* is the predicting magnitude, C is the curvature parameter, q is the quality index, A (in 10^9 $J^{1/2}$) is the parameter of the power-law relation (1), R (in km) is the radius of the circular critical regions (or the radius of the circle with area equal to the area of the elliptical regions for cases 8,10,11,12), $\mathbf{M}_{13}$ is the average magnitude of the three largest preshocks, S_r (in $J^{1/2}$/yr) is the long-term Benioff strain rate in the critical region, s_r is the same quantity per $10^4 km^2$, $\mathbf{M}_{min}$ is the smallest preshock magnitude, n is the number of preshocks, t_s the start year of the preshock sequence, t_i is the identification time.

This relation fits a large sample of data (mainshock magnitude range 4.6–8.6), which concerns elliptical critical regions in the Aegean area as well as data for California and other areas presented by Bowman *et al.* (1998). The values of R and **M*** presented in Table 2 have been used to calculate the values of a_m for each of the twenty mainshocks listed in this table. The mean a_m value for each of the five areas is listed on Table 3, where the corresponding mean deformation rate, s_r (in $J^{1/2}$/yr and per 10^4 km^2) is also given. The plot of a_m as a function of s_r is presented in Figure 8, where a linear relation can be identified ($a_m = 1.38 - 0.32 \log s_r$, $r = -0.95$). Thus, relation (4) becomes:

$$\log R = 0.42\mathbf{M}^* - 0.32\log s_r + 1.38, \quad \sigma = 0.11. \quad (5)$$

This equation suggest that the size of a critical region scales with both the magnitude of the mainshock, **M***, and the long-term rate of seismic crustal deformation, s_r, in the critical region. In particular, this dimension increases with the magnitude of the mainshock but decreases with the rate of seismic crustal deformation. Hence, the size of a critical region, which corresponds to a mainshock of certain magnitude is, for example, smallest for Japan, where the crustal deformation rate is high, larger for Greece, and much larger for Anatolia, California, and the Himalayas (Fig. 8).

Dobrovolsky *et al.* (1979) adopted the model of an elastic soft inclusion in a more rigid elastic space in order to determine the region of precursory deformation for a future earthquake. In their model, they assumed that this region is centered at the epicenter of the oncoming mainshock and showed that the mean radius, r (in km), of the region is related to the magnitude, **M**, of the expected earthquake by the formula:

$$\log r = 0.43\mathbf{M} - 0.33\log \varepsilon - 2.73, \quad \mathbf{M} \geq 5.0 \quad (6)$$

where ε is the greatest principal strain. Comparison of their theoretical results with observations on several precursory phenomena (geochemical, resistance, telluric, radon, light effects) showed that most precursors were observed for distances corresponding to a strain levels, ε, between 10^{-6} and 10^{-8}. The similarity between relation (5), which gives the radius of the critical region, and relation (6), which gives the size of the preparing region, is striking since in both relations the radius scales with the magnitude of the oncoming mainshock and with the deformation measure with almost identical coefficients. Furthermore, by using the values of the parameters a_m of relation (4) given in Table 3, we can obtain the corresponding values of ε (relation 6), which vary be-

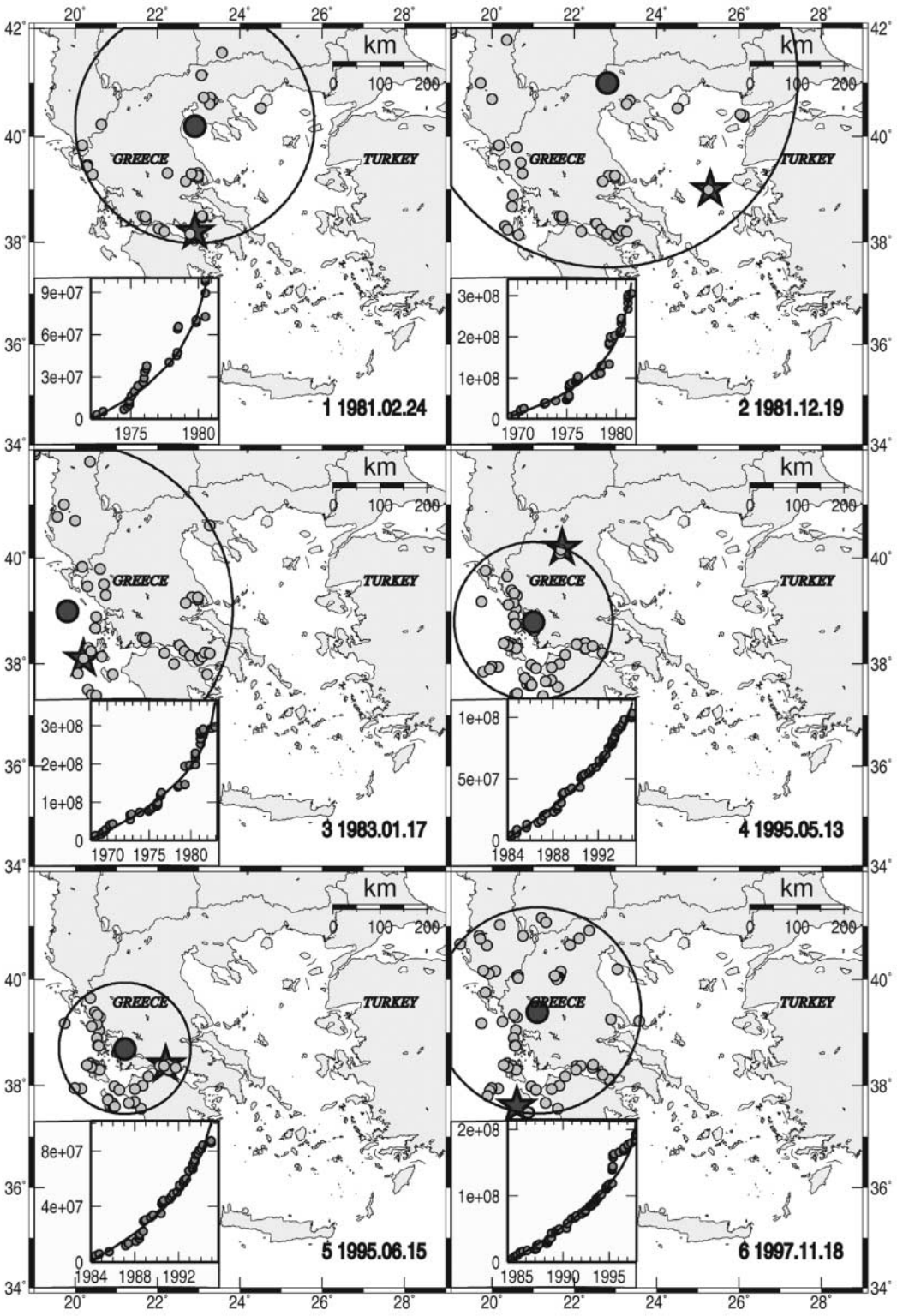

Figure 2. The circular critical regions associated with the preshock accelerating seismic sequences of six mainshocks (**M** ≥6.4) which occurred in Greece. Preshock epicenters are shown by small circles, and the mainshock epicenter is denoted by a star. Numbers and dates correspond to the code numbers and dates in Tables 1 and 2. The inset figures display the time variation of seismic deformation (Benioff strain).

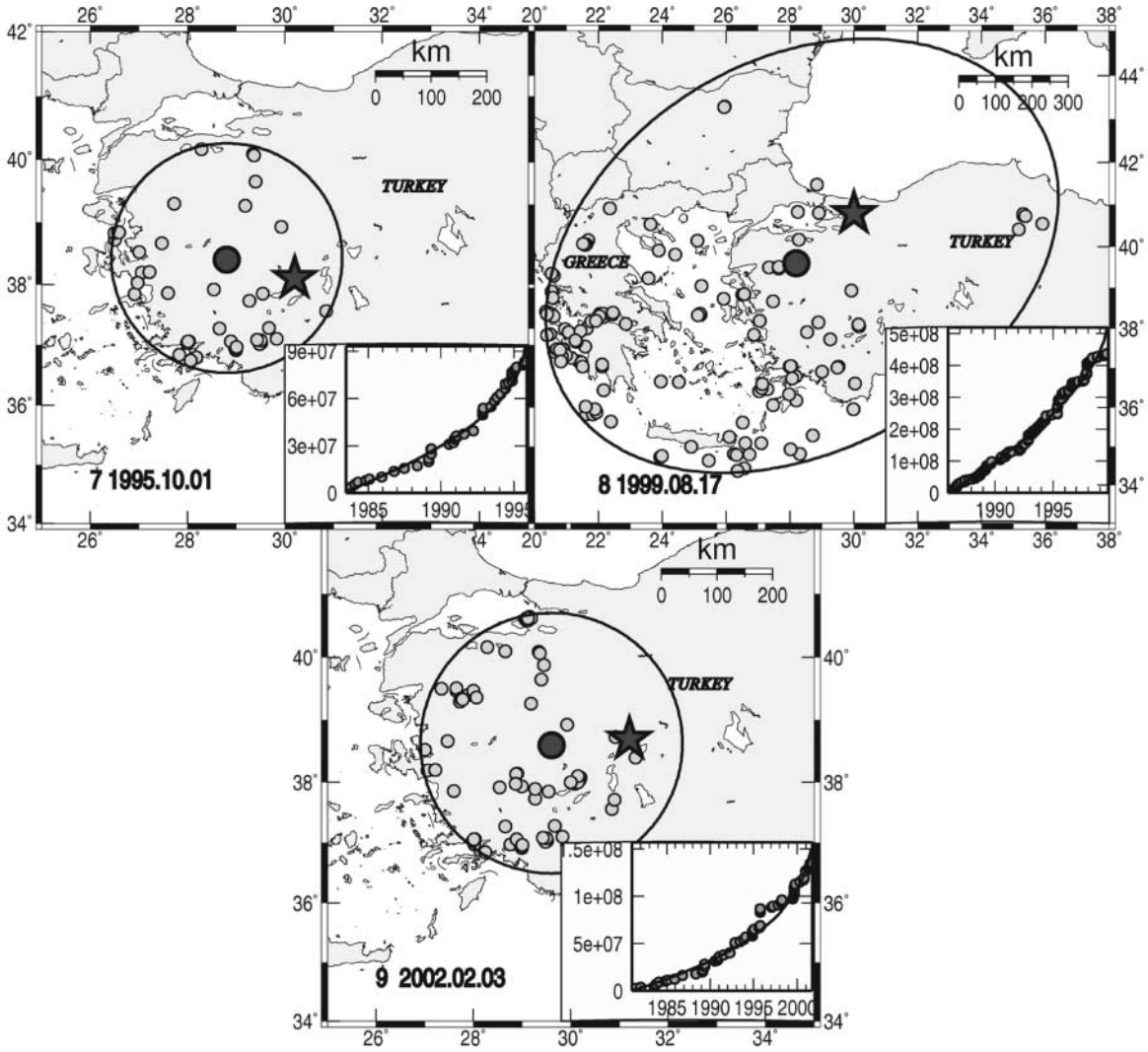

Figure 3. One elliptical and two circular critical regions associated with preshock accelerating seismic sequences of three mainshocks ($\mathbf{M} \geq 6.4$), which occurred in Anatolia (Turkey). Symbols are as in Figure 1.

tween $10^{-6.3}$ and $10^{-7.3}$, in agreement with the values of ε for which precursory phenomena are observed.

The similarity of equations (5) and (6) should take into account that, despite the fact that Benioff strain is a stable quantity to use in similar studies, as early works (e.g., Varnes, 1989; Bufe and Varnes, 1993) have shown, it is difficult to assign a clear physical meaning to Benioff strain owing to its divergence when smaller magnitude events are gradually included. However, Benioff strain is finite if only events above a threshold value (e.g., $\mathbf{M}_{\min}$ in this work) are considered, which are those events that contribute to the accelerated deformation phenomenon examined in the present study (equation 3). In this case and for several models, it can be shown that the Benioff strain is proportional to the classical strain, ε, (e.g., Ben-Zion and Lyakhovsky, 2002), hence $\log s_r$ and $\log \varepsilon$ have a simple constant shift. In any case, the similarity of equations (5) and (6) shows that for a specific model (Dobrovolsky *et al.*, 1979), the scaling relations have a similar dependence not only on the mainshock magnitude but also on the loading/seismicity rate, as is also shown by real data. An important point is that this similarity also suggests that the critical (preshock) region of an oncoming mainshock coincides with its preparing region, where other geophysical precursors are also observed.

Table 3 presents the mean values of the durations, t_p (in years), of the preshock sequence for each of the five areas. The plot of t_p versus s_r in Figure (9) shows that the duration of preshock sequences scales with the rate of seismic crustal deformation according to the relation

$$\log t_p = 3.87 - 0.45 \log s_r, \qquad \sigma = 0.10. \qquad (7)$$

Thus, for Japan (highest s_r values), the duration of the preshock sequence is of the order of 11 years and increases for

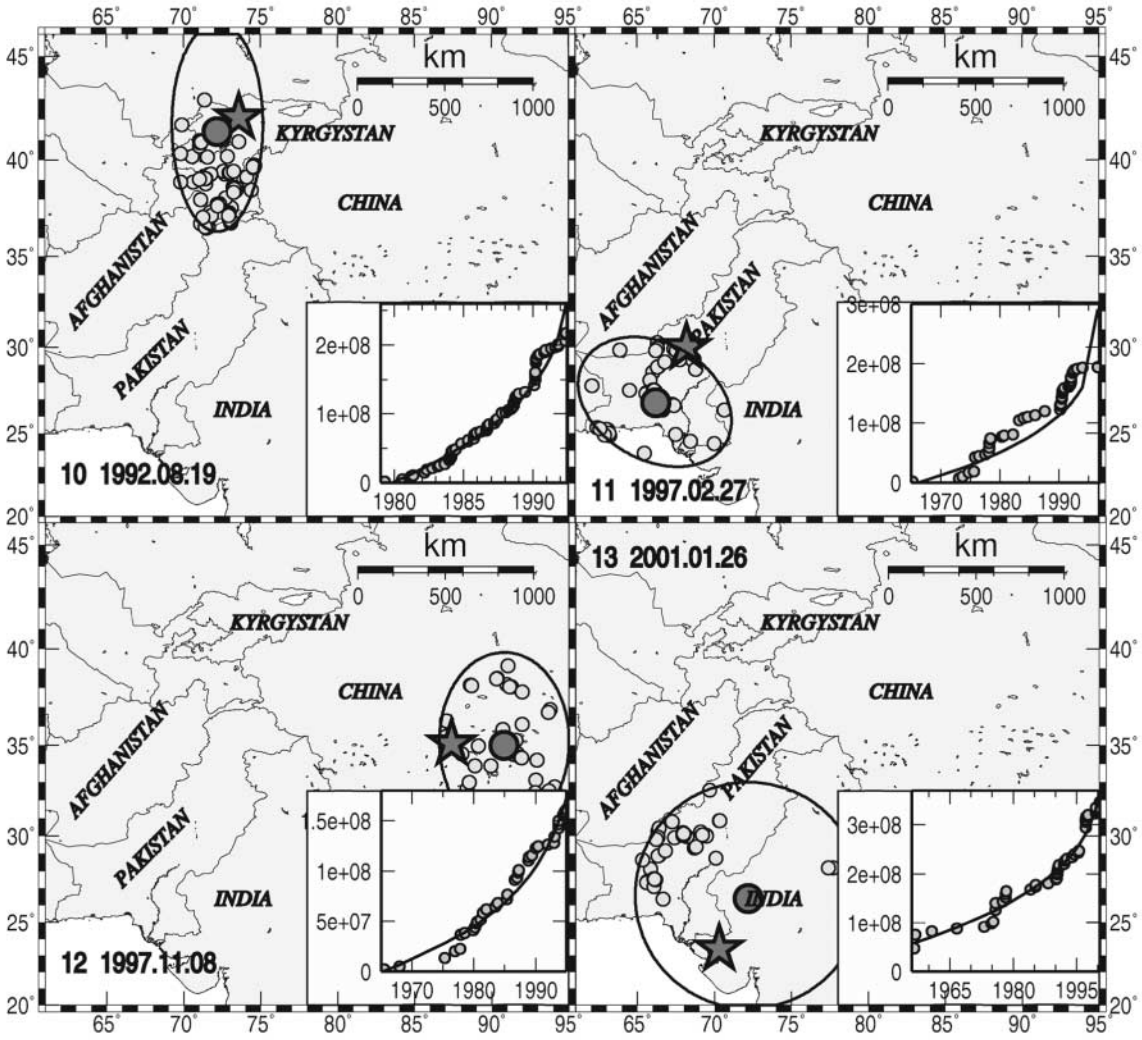

Figure 4. Three elliptical regions and one circular critical region associated with the preshock accelerating seismic sequences of four mainshocks (**M** ≥7.1), which occurred in the Himalayas area; symbols are as in Figure 1.

lower deformation rates, becoming about 13 years for Greece, 15 years for Anatolia, 27 years for California, and 35 years for the Himalayas.

From the values of A, t_p, and S_r presented in Table 2, we find that

$$\log\left(\frac{A}{t_p}\right) = 1.01 \log S_r, \qquad \sigma = 0.04, \tag{8}$$

which is similar to the relation derived for the Aegean area. This relation suggests that the mean rate of deformation, A/t_p, during the accelerating deformation in the critical region is almost equal to the long-term rate of seismic deformation, S_r, in the same critical region.

From the values of $\mathbf{M}^*$ and $\mathbf{M}_{13}$ given in Table 2, the following relation can be derived:

$$\mathbf{M}^* = \mathbf{M}_{13} + 0.60, \qquad \sigma = 0.15. \tag{9}$$

This simple formula constitutes an important constraint to the critical earthquake model and can be used for an independent estimation of the magnitude of an ensuing mainshock. A linear relation between the magnitude of a mainshock and the mean magnitude of the three largest shocks of preshock swarms has also been proposed by Evison and Rhoades (1997).

We should note that the results previously presented were recomputed using the highest q value (equation 2), where the smallest C value is combined with the highest P value, as this is determined from the compatibility of the observed accelerated deformation behavior with the preliminary form of equations (5), (7), (8), and (9). This is clearly seen in Figure 10, where the spatial distribution of the C and Q values is presented for event 15 of Table 1. A much sharper peak of the q value is observed close to the epicenter than of the C value, verifying the usefulness of the q parameter in the search for valid accelerated deformation patterns.

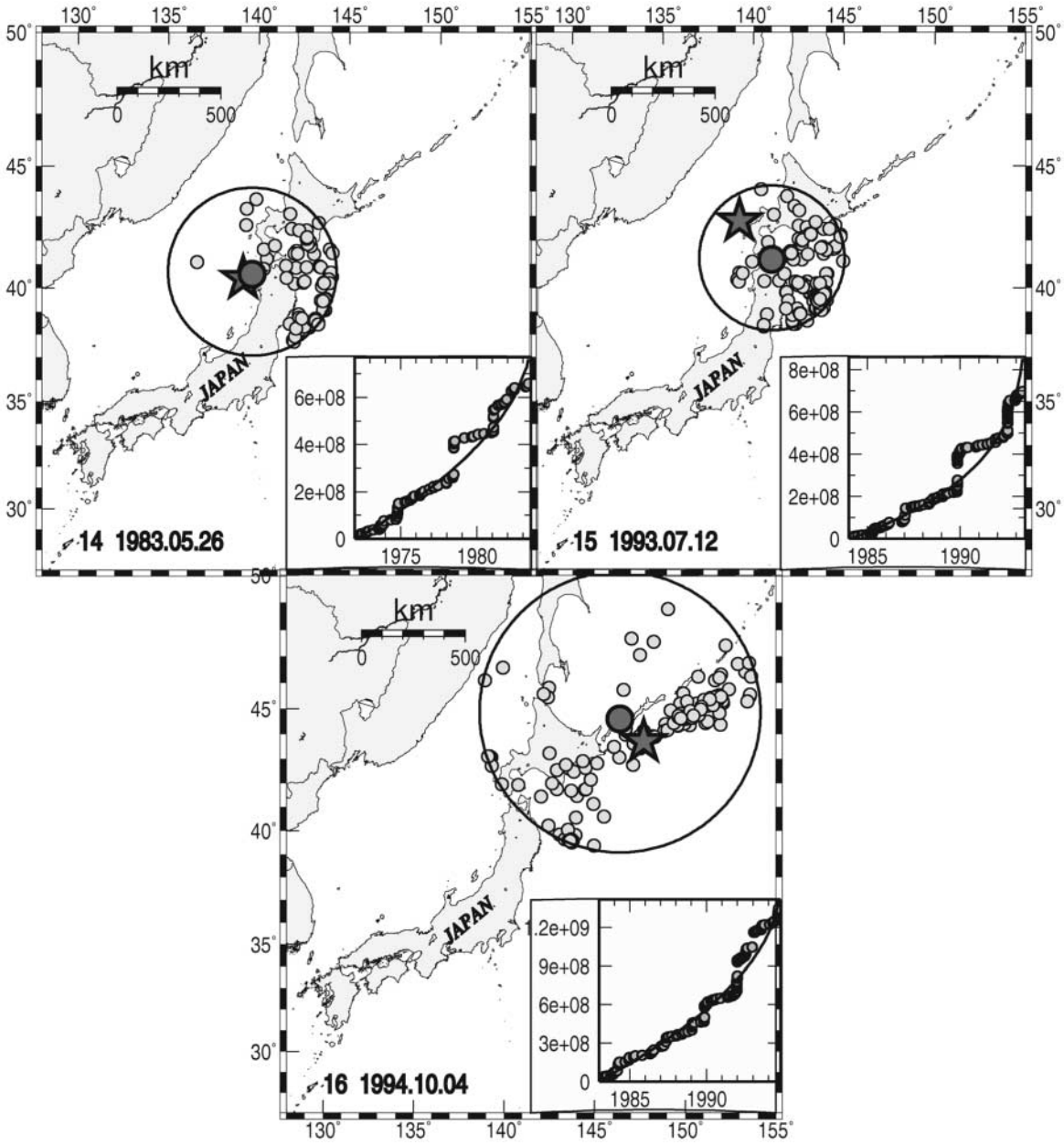

Figure 5. The circular critical regions associated with the preshock accelerating seismic sequences of three mainshocks (**M** ≥7.3), which occurred in Japan; symbols are as in Figure 1.

Valid accelerating seismic deformation ($C < 0.60$, $m = 0.30$) cannot be identified until a certain time, t_i (before the origin time of the mainshock), which can be considered as the identification time. This is the earliest time up to when the available data of a preshock sequence give a valid solution, and it is usually associated with a seismic excitation (Papazachos *et al.*, 2001). To estimate the identification time of a preshock sequence before the generation of the mainshock, the following procedure is applied. Considering several assumed values, T_c, for the unknown origin time of the mainshock (e.g., in steps of 1 month), we let the program try to fit relation (1) to the data until the first valid solution is obtained. At this time, the assumed origin time has a value, T_i, which corresponds to a value, t_i, of the time up to when preshock data have been used and which is the identification time. In the last column of Table 2, the values of t_i determined by this procedure are given for each one of the 20 preshock sequences. From the values of t_i given in Table 2, it is clear that the difference $t_c - t_i$ also scales with the long-term seismicity rate s_r, with a scaling coefficient (slope) similar to the total preshock duration, t_p (relation 7). The scaling coefficient of the corresponding linear relation is -0.43, hence practically identical to that of equation (7), which applies for the total preshock duration. For this rea-

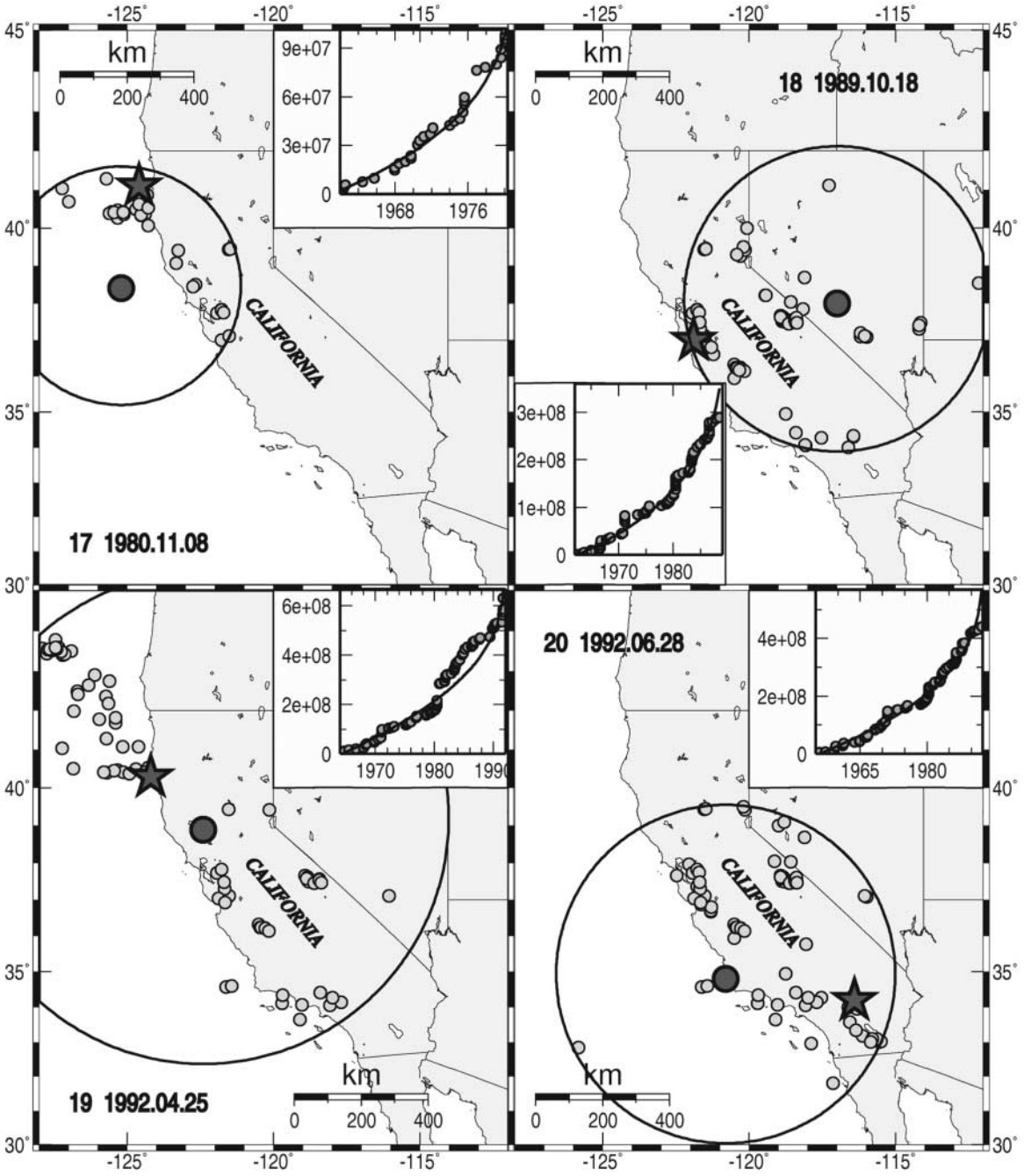

Figure 6. The circular critical regions associated with the preshock accelerating seismic sequences of four mainshocks ($\mathbf{M} \geq 7.0$) in California; symbols are as in Figure 1.

son, we adopted the same scaling coefficient (-0.45), and from the listed values the following relation was obtained:

$$\log(t_c - t_i) = 3.08 - 0.45 \log s_r, \quad \sigma = 0.24. \quad (10)$$

Comparing equation (10) with equation (7) shows that the ratio of the duration of the identification period, $t_c - t_i$, is $\sim$16% of the total duration, t_p, of the preshock sequence, in agreement with previous results concerning preshock sequences in the Aegean area (Papazachos *et al.*, 2002b), as well as with the value (0.17) determined by an independent method and data (Yang *et al.*, 2001). Relation (10) can take the form

$$t_c = t_i + \exp(7.09 - 1.04 \log s_r), \quad \sigma = 1.7 \text{ years}, \quad (11)$$

which can be also used to estimate the origin time, t_c, of an oncoming mainshock.

It is interesting to examine the average distance of the point where the highest q value is observed from the true

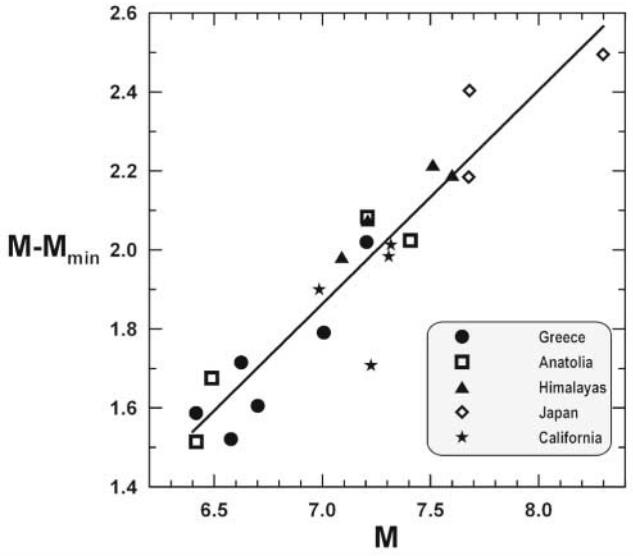

Figure 7. Variation of the difference, $\mathbf{M} - \mathbf{M}_{min}$, of the mainshock magnitude, **M**, and the minimum preshock magnitude, $\mathbf{M}_{min,}$ as a function of **M**, for the $\mathbf{M}_{min}$ value for which the best solution (highest accelerating deformation) is obtained.

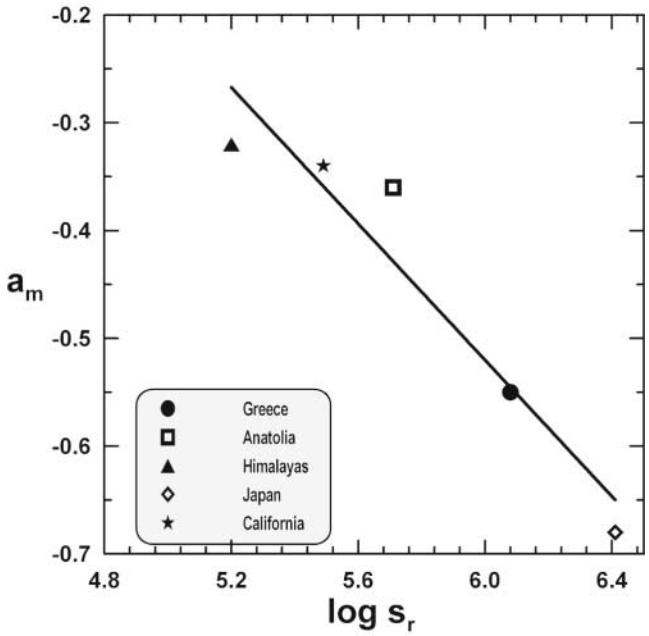

Figure 8. Variation of parameter a_m (relation 5) with the seismic deformation rate, s_r.

Table 3

Mean Values for the Logarithm of the Seismic Deformation Rate, s_r (in $J^{1/2}$ per year and per $10^4 km^2$); the Parameter a_m of Relation (5); and the Duration, t_p (in years) of the Preshock Sequences for Each of the Five Examined Areas

Area	log s_r	a_m	t_p
Greece	6.08 ± 0.19	−0.55 ± 0.03	12.5 ± 2.0
Anatolia	5.71 ± 0.15	−0.36 ± 0.03	15.0 ± 4.3
Himalayas	5.20 ± 0.33	−0.32 ± 0.03	34.8 ± 8.2
Japan	6.41 ± 0.07	−0.68 ± 0.03	11.0 ± 1.0
California	5.49 ± 0.07	−0.34 ± 0.01	27.0 ± 5.3

epicenter. Examination of the available results showed that this distance does not scale with the magnitude of the earthquake but only with the seismicity, as this is expressed by the Benioff strain rate, s_r, according to the relation

$$x = 1150 - 160 \log s_r, \quad \sigma = 60 \text{ km}. \qquad (12)$$

Discussion

In the present work, where properties of preshock sequences of known mainshocks are investigated, the basic parameter used to quantify the accelerating time variation of Benioff strain is the curvature parameter *C*, which expresses the deviation from linearity and the degree of acceleration. Thus, the small positive values of C (≤ 0.60) observed for all 20 preshock sequences, which occurred in a variety of seismotectonic regimes, indicate that this accelerating seismicity is a systematic premonitory pattern.

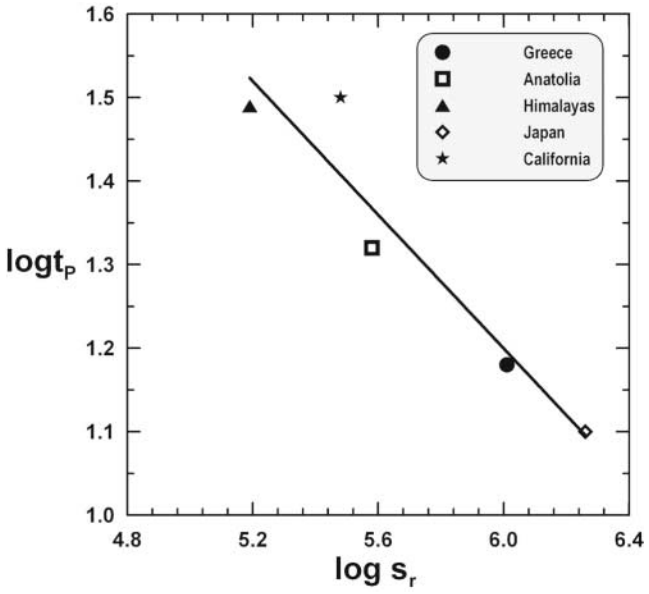

Figure 9. Variation of the duration, t_p, of the preshock sequence with the seismic deformation (Beniof strain rate), s_r.

The fitting of the data by a power law with a power value ($m = 0.3$) predicted by theory and the excellent agreement between the empirically derived scaling relation of the spatial dimension of the critical region (relation 5) with a theoretically obtained relation (6) give support to the critical earthquake model and a physical meaning to the preshock accelerating seismicity.

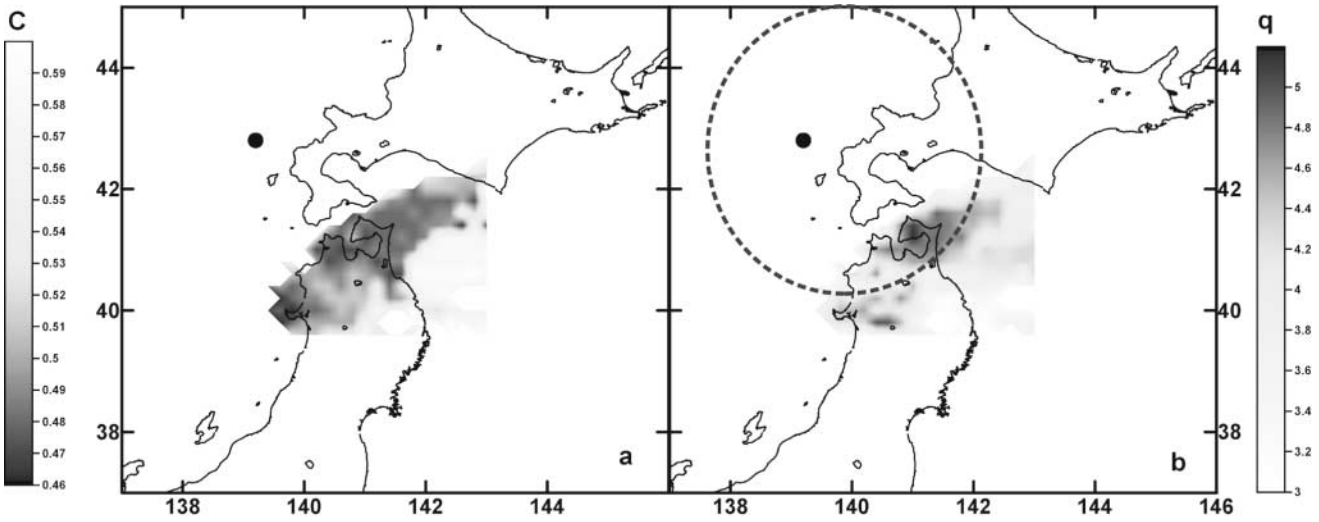

Figure 10. Comparison of the spatial variation of the C (a) and q (b) values for the 1993 **M** 7.7 Hokkaido Nansei-Oki earthquake in Japan (event 15 in Table 1). A much sharper high-value peak close to the epicenter (solid circle) is observed for the q distribution.

The results of the present work can be of importance for intermediate-term earthquake prediction research, because the magnitude, the origin time, and their uncertainties for an oncoming mainshock can be estimated by relations that express properties of the critical earthquake model. By such relations, useful information can also be obtained for the epicenter of an oncoming mainshock, which can lead to the estimation of the epicenter coordinates and their uncertainties, in combination with other data.

The magnitude of an ensuing mainshock can be estimated by relations (5) and (9). Comparison of the magnitudes estimated by this method (**M*** in Table 2) with observed magnitudes (**M** in Table 1) shows differences ranging between -0.4 and 0.4, with a mean difference about zero and a standard deviation of 0.22. This result indicates that the magnitude of an oncoming mainshock can probably be estimated with a maximum error of $\pm$ 0.4 with a high confidence ($\sim$ 95%).

Relations (10) and (11) can be used to estimate the origin time of an ensuing mainshock because the identification time, t_i, can be estimated from properties of the preshock sequence. The uncertainties in these relations ($\sigma = 1.7$ yrs) indicate that the origin time of the ensuing mainshock can probably be estimated by this method with an error of ± 3.4 yrs with high confidence ($\sim$95%).

It should be pointed out that there are a few additional events in the specific time–magnitude–space windows previously defined for each study area, for which results are not presented in this work. In most cases (e.g., five cases in Greece, one in Anatolia, and one in Japan), these events are normal aftershocks or foreshocks (one case in Greece), where the process is controlled by the mainshock and no accelerated deformation pattern can be identified and separated for these events. The same is true for the 16 October 1999, **M** 7.1, Hector Mine event in California, which can be considered as a late aftershock of the Landers 1992, **M** 7.3, mainshock. Moreover, no identification of accelerated deformation was possible for the 28 December 1994, **M** 7.7, event, which occurred immediately after the big 4 October 1994, **M** 8.3, Shikotan event in Japan (event 16 in Table 1) within its critical region, as well as for the 1 November 1989, **M** 7.4 event, which again fell in the critical region of the 26 May 1983, **M** 7.7 (event 14 in Table 1), and occurred within a few years after the previous larger event (**M** 7.7) within its critical region. Hence, it appears that it is impossible to identify an accelerated deformation pattern for smaller magnitude events within the critical region or for a few years after the generation of a large mainshock such as the big Shikotan 1994 event, as the pattern of the mainshock dominates and does not allow the grid-search algorithm to identify and separate the phenomena for the later, smaller magnitude event. This observation sets a limit on the possible predictive ability of the described pattern, as the method is blind for a few years after the generation of a large mainshock, at least within its critical region.

The information given in the present work shows that identification of accelerated deformation is not enough for locating the epicenter of an oncoming mainshock, with a reasonable accuracy, since the epicenter tends to lie at a distance (equation 12) from the best solution (point Q). Similar results have been obtained by other researchers (Robinson, 2000), who have examined cases where the center of the critical region (maximum q value in our grid search) does not coincide with the mainchock epicenter. A possible physical explanation for this bias (relation 12) could be the fact that a large number of observations suggest that decelerating seismic deformation (quiescence) occurs in the narrower rupture zone of an ensuing mainshock (Wyss *et al.*, 1981;

Wyss and Habermann, 1988; Hainzl *et al.*, 2000; Zoller *et al.*, 2002; Papazachos *et al.*, 2005). Thus, the epicenter zone of the mainshock where decelerating deformation occurs during the critical period has the tendency to push the best solution obtained from the grid-search algorithm away from the center of the region where accelerating deformation occurs (see Fig. 10), as this is seen by relation (12). This is clearly seen in Figure 11, where the variation of the cumulative Benioff strain is shown for the same event examined in Figure 10, for a narrower seismogenic source area (elliptical region in Fig. 10). A clearly decelerating pattern is observed, and we can easily apply equation (1) with an exponent $m > 1$ in an attempt to model this decelerating (quiescence) behavior. This observation and equation (12) suggest that the results obtained in this work should be combined with independent information (decelerating seismicity in the rupture zone, location of active faults, etc.) to locate the epicenter of an oncoming mainshock with a higher accuracy.

The procedure followed in the present work must be applied to future mainshocks in order to test its capability more objectively. It must be noticed that the identification of the critical region of an ensuing mainshock has to be based on the spatial distribution of the values of the quality parameter $q(= P/[C^*m])$, because it expresses the degree of accelerating seismicity (through C), the degree of fit of observations to a power law (through m), and the degree of agreement of properties of the examined region to preshock properties expressed by relations (5, 7, 8, and 9) through P.

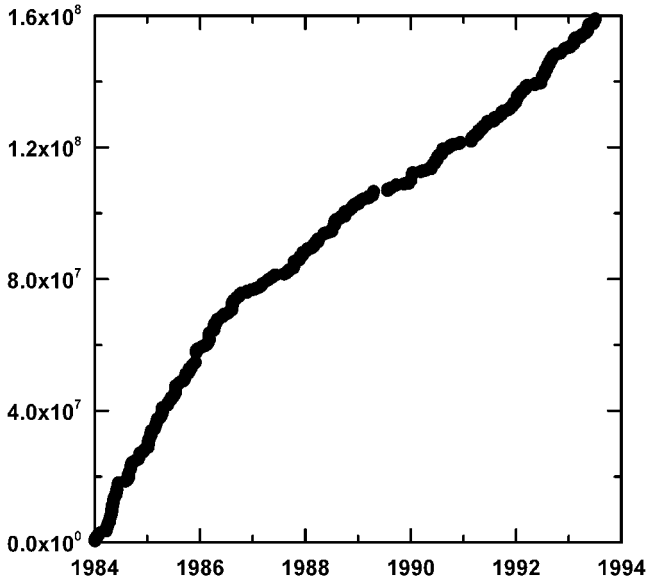

Figure 11. Variation of the cumulative Benioff strain for the narrower seismogenic source region of the 1993 **M** 7.7 Hokkaido Nansei-Oki earthquake in Japan (elliptical area in Fig. 10). A clear decelerating pattern is observed, in contrast to the accelerating deformation pattern of the broader critical region (circular area in the upper right part of Fig. 5).

We should also point out that the critical region of an oncoming mainshock, where a preshock accelerating deformation is observed, coincides with the preparing region for this earthquake, where other precursory phenomena are observed. This is of importance from a practical point of view, because these regions, which are easily defined by the method presented in the present article, can be searched to identify other precursors of oncoming mainshocks.

Acknowledgments

We would like to thank two anonymous reviewers for their constructive comments and suggestions, which helped to improve our work. Thanks are also due to Wessel and Smith (1995) for their generous distribution of the GMT software, which was used to generate some of the figures of this study. This work has been partly financed by the Greek Earthquake Planning & Protection Organization (OASP) under project 20242 and the Pythagoras EPEAEK project 21945 Aristotle Univ. Thessaloniki Research Committee, and it is Geophysical Lab. Univ. Thessaloniki contribution #631/2003.

References

Allegre, C. J., and J. L. Le Mouel (1994). Introduction of scaling techniques in brittle failure of rocks, *Phys. Earth Planet. Interiors* **87,** 85–93.

Andersen, J. V., D. Sornette, and K. T. Leung (1997). Tri-critical behavior in rupture induced by disorder, *Phys. Rev. Lett.* **78,** 2140–2143.

Ben-Zion, Y., K. Dahmen, V. Lyakhovsky, D. Ertas, and A. Agnon 1999. Self-driven mode switching of earthquake activity on a fault system. *Earth Planet. Sci. Lett.* **172,** 11–21.

Ben-Zion, Y., and V. Lyakhovsky (2002). Accelerated seismic release and related aspects of seismicity patterns on earthquake faults, *Pure Appl. Geophys.* **159,** 2385–2412.

Bowman, D. D., G. Quillon, C. G. Sammis, A. Sornette, and D. Sornette (1998). An observational test of the critical earthquake concept, *J. Geophys. Res.* **103,** no. 24, 372.

Bowman, D. D., and G. C. King (2001). Stress transfer and seismicity changes before large earthquakes, CR *Acad. Sci.*, Series IIA, *Earth Planet. Sci.* **333,** 591–599.

Brehm, D. J., and L. W. Braile (1998). Intermediate-term earthquake prediction using precursory events in the New Madrid seismic zone, *Bull. Seism. Soc. Am.* **103,** 24,359–24,372.

Brehm, D. J., and L. W. Braile (1999). Refinement of the modified time-to-failure method for intermediate-term earthquake prediction, *J. Seism.* **3,** 121–138.

Bufe, C. G., and D. J. Varnes (1993). Predictive modeling of seismic cycle of the greater San Francisco Bay region, *J. Geophys. Res.* **98,** 9871–9883.

Dobrovolsky, J. P., S. I. Zubkov, and B. J. Miachkin (1979). Estimation of the size of earthquake preparation zones, *Pure Appl. Geophys.* **117,** 1025–1044.

Evison, F. F., and D. A. Rhoades (1997). The precursory earthquake swarm in New Zealand. *N.Z. J. Geol. Geophys.* **40,** 537–547.

Felzer, K. R., T. W. Becker, R. E. Abercrombie, G. Ekstrom, and J. R. Rice (2002). Triggering of the 1999 M_w 7.1 Hector Mine earthquake by aftershocks of the 1992 M_w 7.3 Landers earthquake. *J. Geophys. Res.* **107,** 2190, doi 10.1029/2001JB000911.

Gross, S., and J. Rundle (1998). A systematic test of the time-to-failure analysis, *Geophys. J. Int.* **133,** 57–64.

Guarino, A. S., S. Ciliberto, and A. Garcimartin (1999). Failure time and microcrack nucleation, *Europhys. Lett.* **47,** 456–461.

Guarino, A. S., S. Ciliberto, A. Garcimartin, M. Zei, and R. Scorretti (2002). Failure time and critical behaviour of fracture precursors in heterogeneous materials, *Eur. Phys. J.* **26,** 141–151.

Harvard Seismology (2005). CMT catalog, www.seismology.harvard.edu/CMTsearch.html.

Hainzl, S., G. Zoller, J. Kurths, and J. Zschau (2000). Seismic quiescence as an indicator for large earthquakes in a system of self-organized criticality, *Geophys. Res. Lett.* **27,** 597–600.

International Seismological Centre, (2005). On-line Bulletin, www.isc.ac.uk/Bulletin/rectang.htm Thatcham Thatcham, United Kingdom.

Jaume, S. C., and L. R. Sykes (1999). Evolving towards a critical point: a review of accelerating seismic moment/energy release rate prior to large and great earthquakes, *Pure Appl. Geophys.* **155,** 279–306.

Jaume, S. C. (2000). Changes in earthquake size–frequency distributions underlying accelerating seismic moment/energy release, *AGU Geophysical Monograph Series* **120,** 199–210.

Johansen, A., and D. Sornette (2000). Critical ruptures, *Eur. Phys. J.* **B18,** 163–181.

Karakaisis, G. F., C. B. Papazachos, A. S. Savvaidis, and B. C. Papazachos (2002). Accelerating seismic crustal deformation in the North Aegean Trough, Greece, *Geophys. J. Int.* **148,** 1–16.

Karnik, V. (1996). *Seismicity of Europe and the Mediterranean*, Publ. of Geophysical Institute of Praha, Academy of Sciences of the Czech Republic, K. Klima (Editor), Praha.

Knopoff, L., T. Levshina, V. J. Keillis-Borok, and C. Mattoni (1996). Increased long-rang intermediate-magnitude earthquake activity prior to strong earthquakes in California, *J. Geophys. Res.* **101,** 5779–5796.

Lamaignere, L., F. Carmona, and D. Sornette (1996). Experimental realization of critical thermal fuse rupture, *Phys. Res. Lett.* **77,** 2738–2741.

Mogi, K. (1969). Some features of the recent seismic activity in and near Japan. II. Activity before and after great earthquakes, *Bull. Earthquake Res. Inst. Univ. Tokyo* **47,** 395–417.

National Earthquake Information Center (2005). USGS, Earthquake Hazards Program (http://neic.usgs.gov/neis/epic/epic.html, http://neic.usgs.gov/neis/sopar/sopar.html).

Papazachos, B. C., and C. B. Papazachos (2000). Accelerated preshock deformation of broad regions in the Aegean area, *Pure Appl. Geophys.* **157,** 1663–1681.

Papazachos, B. C., P. E. Comninakis, G. F. Karakaisis, Ch. A. Papaioannou, C. B. Papazachos, and E. M. Scordilis (2003). A catalogue of earthquakes in Greece and surrounding area for the period 550 BC–2002. *Publ. Geophys. Lab. Univ. Thessaloniki*.

Papazachos, B. C., G. F. Karakaisis, C. B. Papazachos, E. M. Scordilis, and A. S. Savaidis (2001). A method for estimating the origin time of an ensuing mainshock by observations of preshock crustal seismic deformation, in *Proc. 9th International Congress Geol. Soc. Greece*, Athens, 20–25 September 2001, **4,** 1573–1582.

Papazachos, C. B. (2001). An algorithm of intermediate-term earthquake prediction using a model of accelerating seismic deformation. *Second Hellenic Conference on Earthquake Engineering and Engineering Seismology*, 28–30 November 2001, 107–115.

Papazachos, C. B. (2003). Minimum preshock magnitude in critical regions of accelerating seismic crustal deformation. *Bolletino Geofisica Teorica Applicata* **44,** 103–113.

Papazachos, C. B., and B. C. Papazachos (2001). Precursory accelerating Benioff strain in the Aegean area, *Ann. Geofisica* **144,** 461–474.

Papazachos, C. B., G. F. Karakaisis, A. S. Savaidis, and B. C. Papazachos (2002a). Accelerating seismic crustal deformation in the southern Aegean area. *Bull. Seism. Soc. Am.* **92,** 570–580.

Papazachos, C. B., G. F. Karakaisis, and E. M. Scordilis (2002b). Results of retrospective prediction of past strong mainshocks in the broader Aegean region by application of the accelerating seismic deformation method, *Proc. of the 38th ESC Gen. Assoc.*, 1–6 September 2002, Genoa, Italy, 14 pp.

Papazachos, C. B., E. M. Scordilis, G. F. Karakaisis, and B. C. Papazachos (2005). Decelerating preshock seismic deformation in fault regions during critical periods, *Bull. Geol. Soc. Greece* **36,** 1491–1498.

Quillon, G., and D. Sornette (2000). The critical earthquake concept applied to mine rockbursts with time-to-failure analysis, *Geophys. J. Int.* **143,** 454–468.

Robinson, R. (2000). A test of the precursory accelerating moment release model on some recent New Zealand earthquakes, *Geophys. J. Int.* **140,** 568–576.

Rundle, J. B., W. Klein, D. L. Turcotte, and B. D. Malamud (2000). Precursory seismic activation and critical point phenomena. *Pure Appl. Geophys.* **157,** 2165–2182.

Rundle, J. B., D. L. Turcotte, R. Shcherbakov, W. Klein, and C. Sammis (2003). Statistical physics approach to understanding the multiscale dynamics of earthquake fault systems, *Rev. Geophys.* **41,** 1019–1048.

Scordilis, E. M. (2005). Empirical global relations converting M_S and m_b to moment magnitude, *J. Seism.* (in press).

Scordilis, E. M., C. B. Papazachos, G. F. Karakaisis, and V. G. Karakostas (2004). Accelerating seismic crustal deformation before strong mainshocks in the Adriatic and its importance for earthquake prediction, *J. Seism.* **8,** 57–70.

Sornette, A., and D. Sornette (1990). Earthquake rupture as a critical point. Consequences for telluric precursors, *Tectonophysics* **179,** 327–334.

Sornette, D., and C. G. Sammis (1995). Complex critical exponents from renormalization group theory of earthquakes: implications for earthquake predictions, *Journal de Physique I France* **5,** 607–619.

Sykes, L. R., and S. C. Jaume (1990). Seismic activity on neighboring faults as a long term precursor to large earthquakes in the San Francisco Bay area, *Nature* **348,** 595–599.

Tocher, D. (1959). Seismic history of the San Francisco Bay region, Calif. Div. Mines Spec. Rept. 57, 39–48.

Tzanis, A., F. Vallianatos, and K. Makropoulos (2000). Seismic and electric precursors to the 17 January 1983, *M*7 Kefallinia earthquake, Greece: signatures of a SOC system, *Phys. Chem. Earth* **25,** 281–287.

Vanneste, C., and D. Sornette (1992). Dynamics of rupture in thermal fuse models, *Journal de Physique I France* **2,** 1621–1644.

Varnes, D. J. (1989). Predicting earthquakes by analyzing accelerating precursory seismic activity, *Pure Appl. Geophys.* **130,** 661–686.

Wessel, P., and W. Smith (1995). New version of the Generic Mapping Tools, *EOS* **76,** 329.

Yang, W., D. Vere-Jones, and M. Li (2001). A proposed method for locating the critical point of a future earthquake using the critical earthquake concept, *J. Geophys. Res.* **106,** 4121–4128.

Wyss, M., F. Klein, and A. C. Johnston (1981). Precursors of the Kalapana $M = 7.2$ earthquake, *J. Geophys. Res.* **86,** 3881–3900.

Wyss, M., and R. E. Habermann (1988). Precursory seismic quiescence, *Pure Appl. Geophys.* **126,** 319–332.

Zoller, G., and S. Hainzl (2002). A systematic spatiotemporal test of the critical point hypothesis for large earthquakes, *Geophys. Res. Lett.* **29,** 53–57.

Zoller, G., S. Hainzl, and J. Kurths (2001). Observation of growing correlation length as an indicator for critical point behavior prior to large earthquakes, *J. Geophys. Res.* **106,** 2167–2176.

Zoller, G., S. Hainzl, J. Kurths, and J. Zschau (2002). A systematic test on precursory seismic quiescence in Armenia, *Nat. Hazards* **26,** 245–263.

Geophysical Laboratory
University of Thessaloniki
P.O. Box 352-1, GR-54124
Thessaloniki, Greece

Manuscript received 1 September 2004.